Supplementary Material

1 SUPPLEMENTARY FIGURES AND TABLES

1.1 Figures

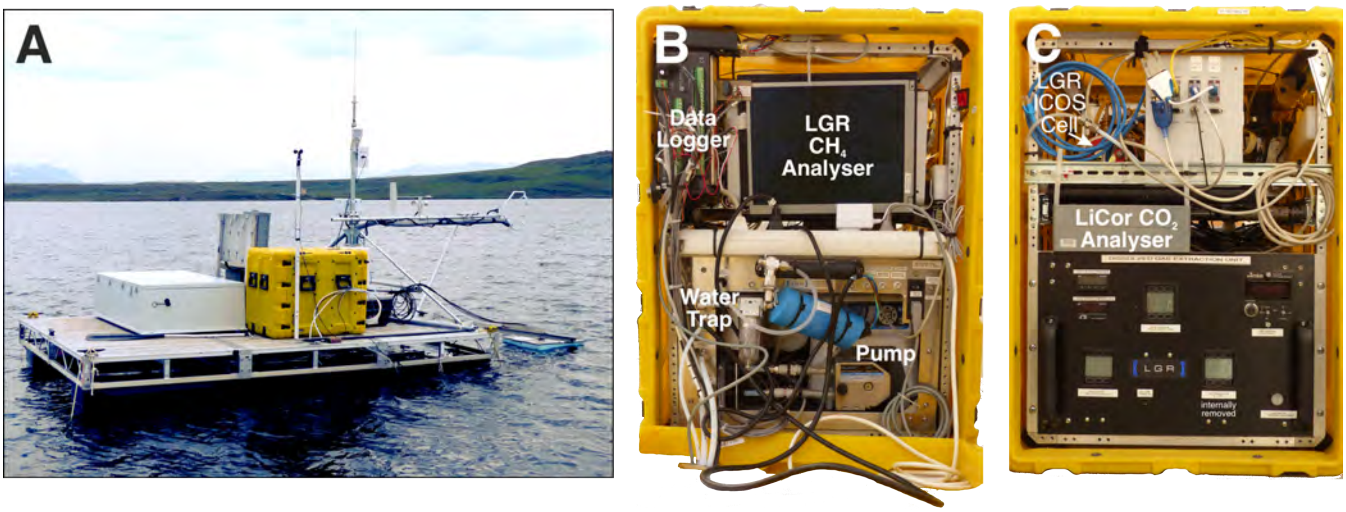

Figure S1. The equilibrator system used during the 2015 ice-off season at Toolik lake. **(A)** Deployment of the equilibrator system on the eddy covariance flux platform. **(B)** Front side with the screen of the LGR methane analyser (hides the analyser itself) in the upper half of the enclosure, and the peristaltic pump with its internal water trap and filter in the lower half. **(C)** Backside with the prototype LGR control unit (at bottom) on which the Licor 820 CO_2 analyser is strapped. The cup anemometer attached to the equilibrator enclosure in **(A)** provided the horizontal wind speed measurements used to calculate the k_{600} piston velocity to derive flux estimates from the measured gas gradients across the water–air interface. The data logger in (A) recorded ancillary analog sensors and the signal from the cup anemometer. The digitized readings where then transferred via a RS-232 serial data line to a Raspberry Pi embedded Linux computer (not visible in **(C)**) that also collected the digital signals of the LGR CH_4 analyser and the LiCor 820 sensor (see USB-to-RS232 interfaces in upper part in **(C)**).

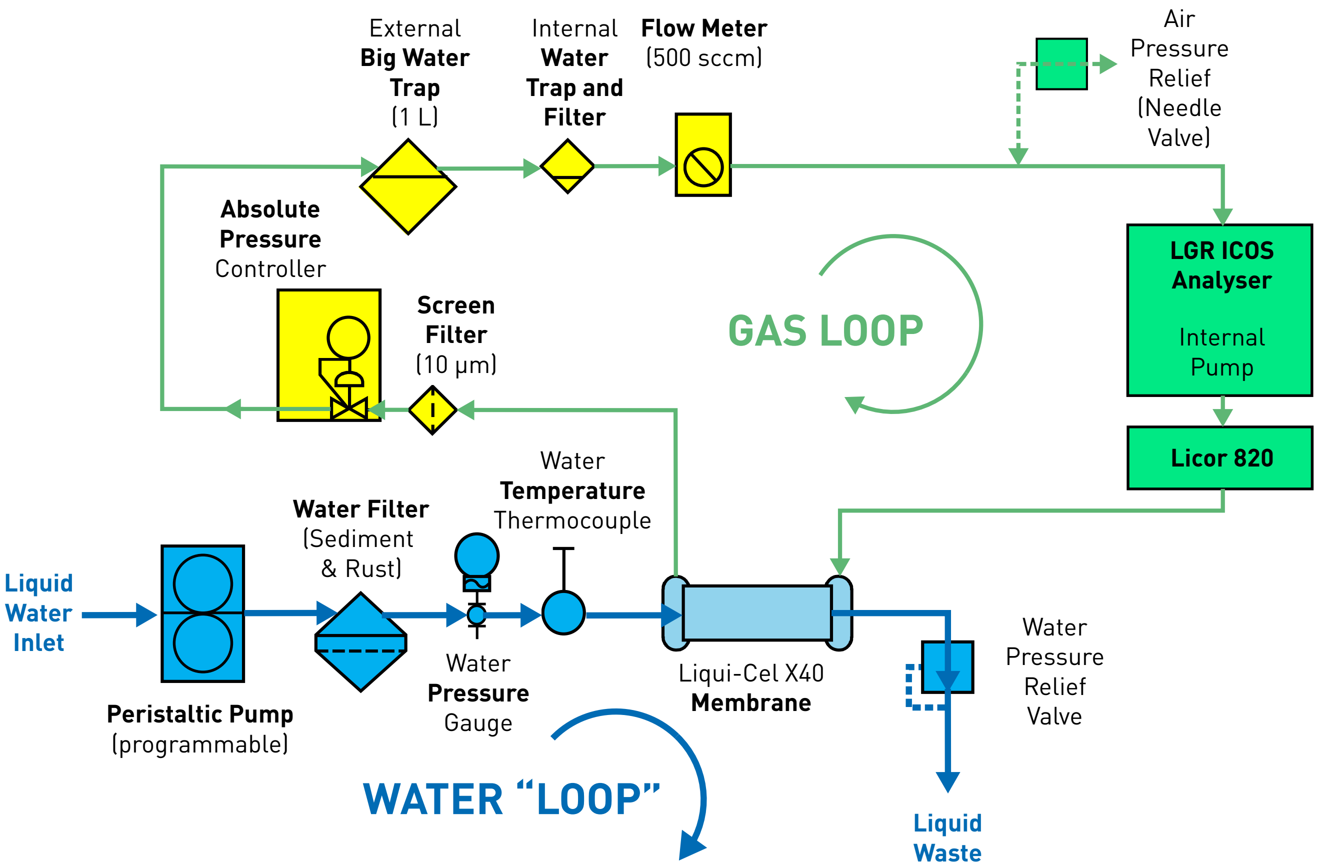

Figure S2. Plumbing scheme of the equilibrator system used during the 2015 ice-off season at Toolik lake. Note that with this plumbing the original gas waste outlet was removed and replaced with a manual needle walve. Original scheme taken from LGR user manual, to use the same symbols for reference.

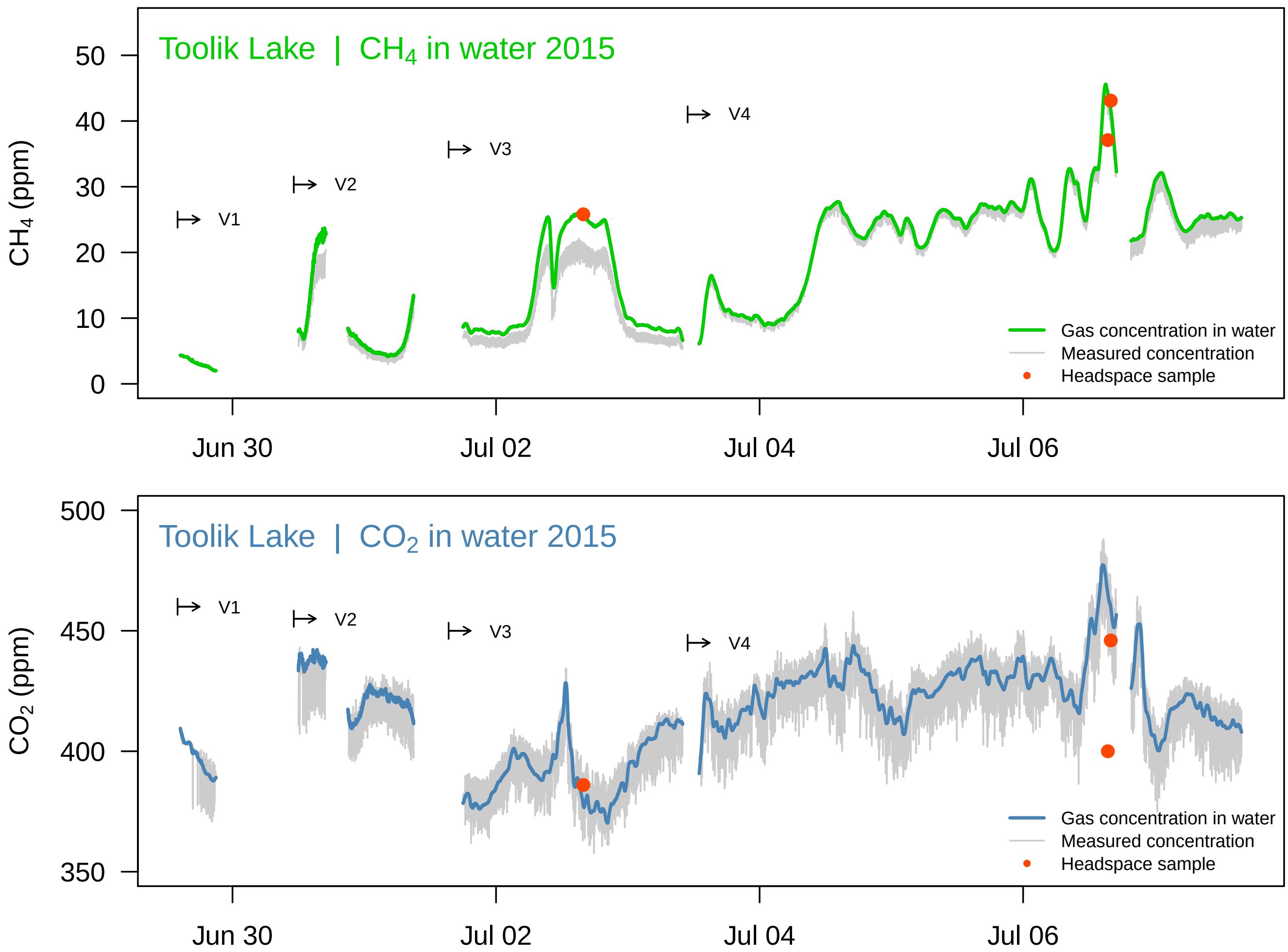

Figure S3. Fine tuning of the equilibrator system after deployment on Toolik lake at the beginning of the ice-off season 2015. Gray solid line shows the measured raw concentrations, and green and blue lines show the final equilibrium concentration calculated with Eq. (1). Four improvements (V1 to V4) were applied, and the equilibrator concentration was compared with three independent headspace equilibration samples (red dots; each dot is the mean of 3 replications). V1: The water trap drop separator (Figure S1B) was already filled after 14 hours. V2: Adjusted liquid water pressure solved the issue with the water trap filling too quickly, but CO_2 concentrations were too high because the LiCor 820 CO_2 analyser was first in line and thus operation at too much underpressure outside the instruments's specification. V3: The configuration was modified to what is shown in Figure S2 with the the LiCor 820 CO_2 analyser after the LGR ICOS analyser. V4: Change of main inlet filter after which the configuration of the equilibrator system was no longer modified until the end of the season.

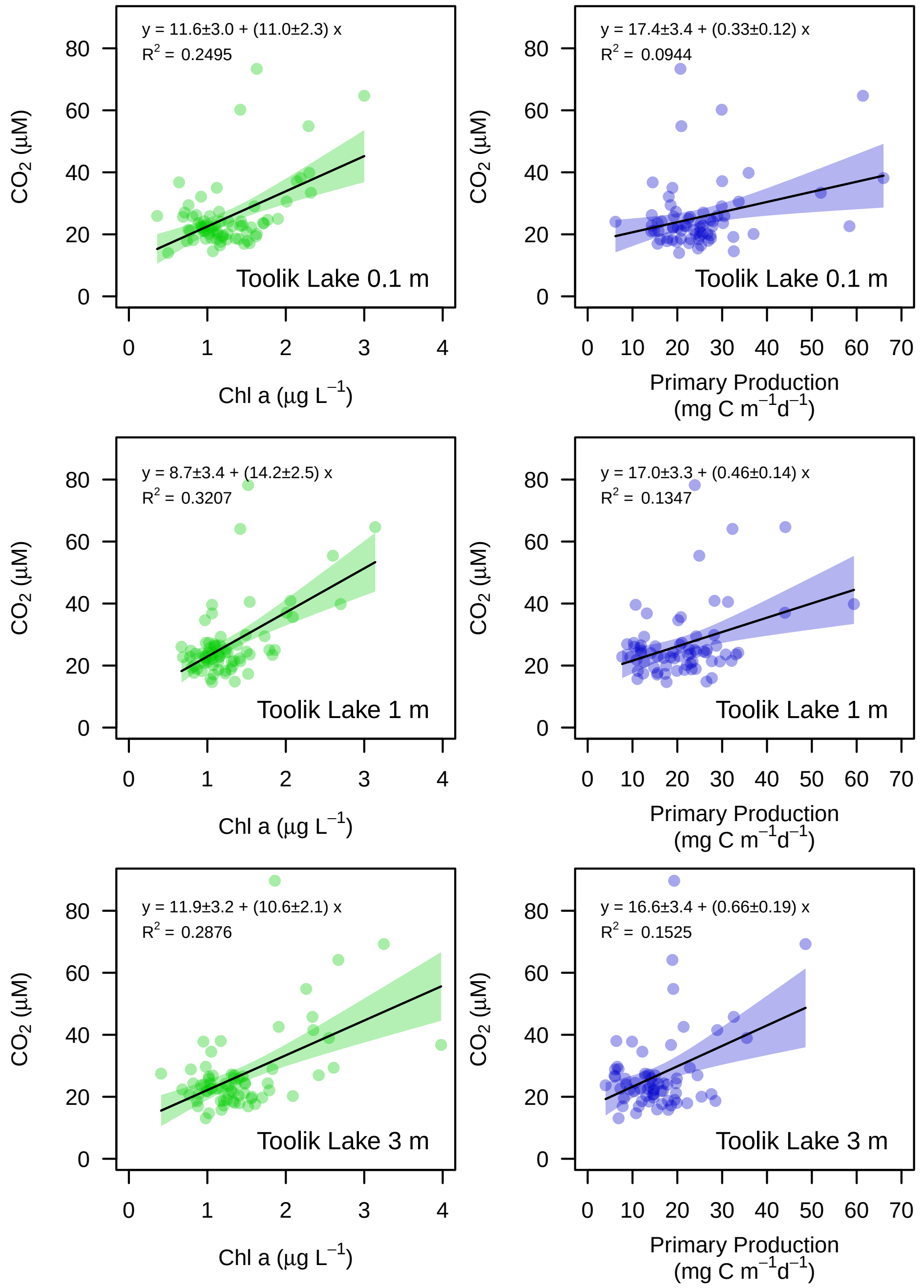

Figure S4. Increasing water CO_2 concentration as a function of chlorophyll a content (left column) and primary production (right column), measured at depths of 0.1 m, 1 m, and 3 m during the ice-free seasons 2010–2021. This indicates that there is no contribution of photosynthesis to the drawdown of CO_2 in Toolik Lake. The color bands show the 95% confidence interval of the respective linear regression fit.

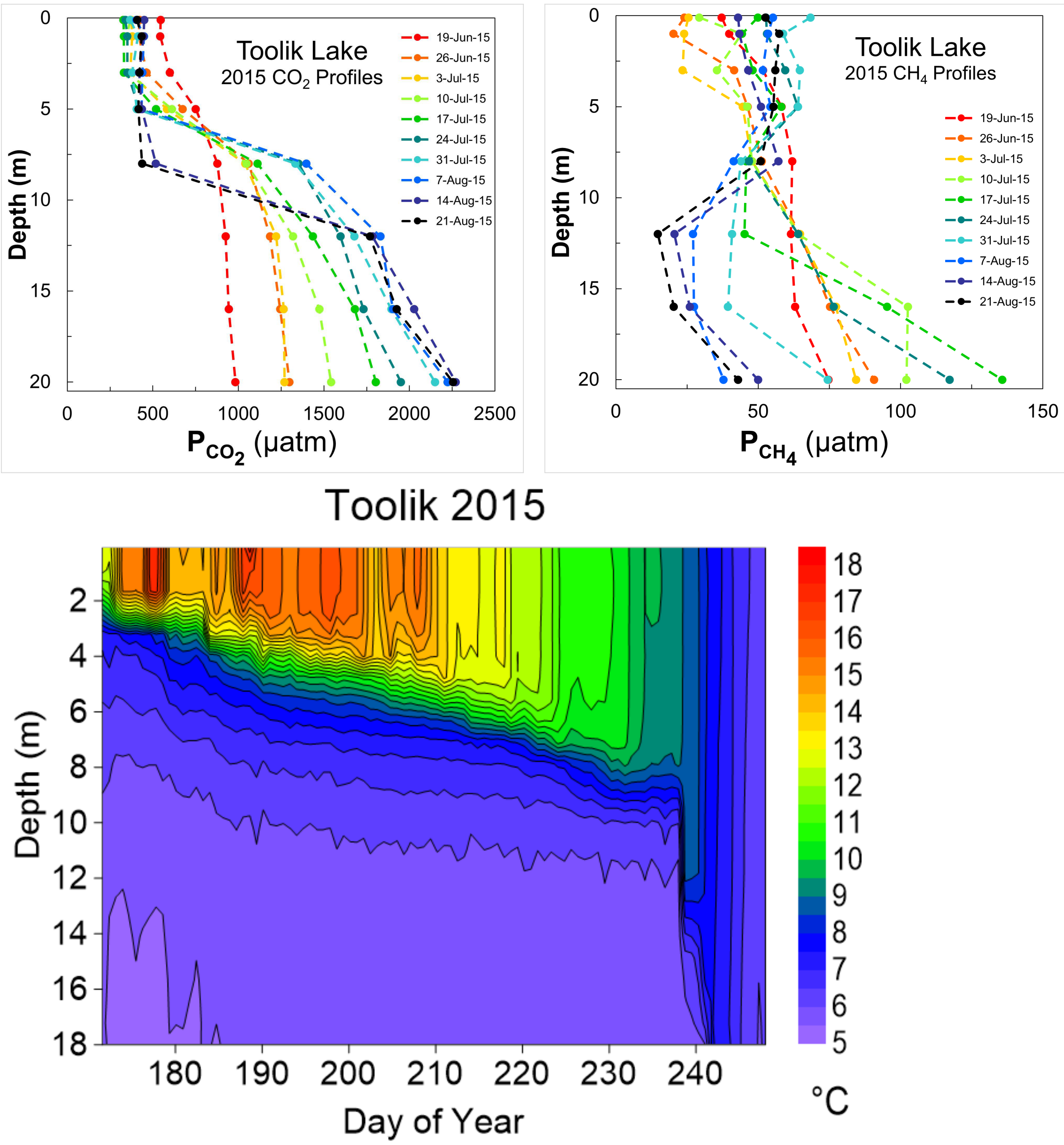

Figure S5. Typical Toolik Lake profiles of CO_2 (top left) and CH_4 (top right) from June to August 2015 (the ice-free season) as determined with the headspace equilibration method. Toolik Lake depth and temperature (bottom) for 2015 from thermistor chain data near the main sampling station.

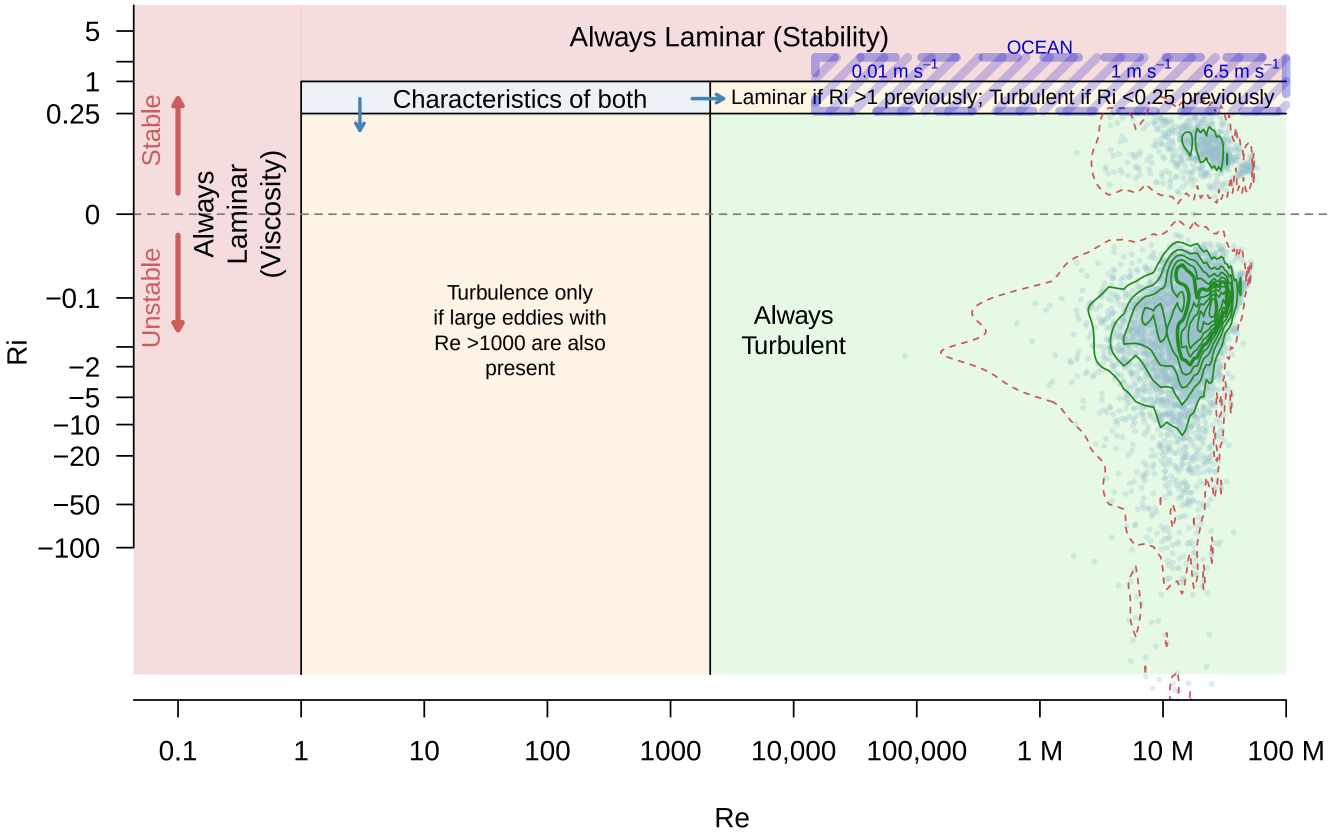

Figure S6. The Richarson number (Ri; atmospheric stability) as a function of the (turbulent) Reynold's number (Re) and turbulence status over Toolik Lake in 2015.

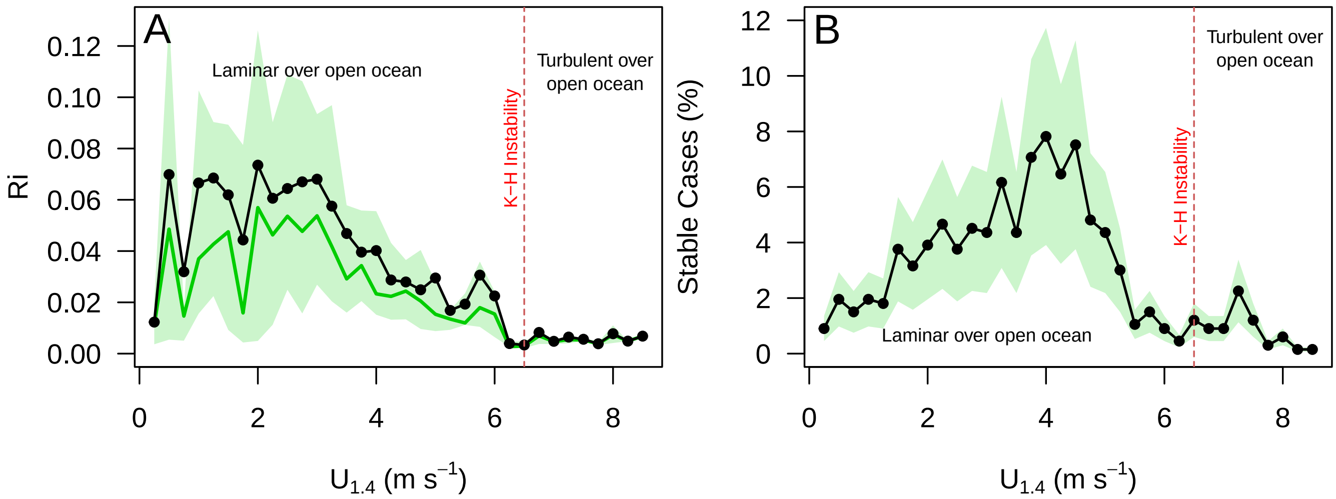

Figure S7. Richardson numbers (**A**; $Ri > 0$) and share of $Ri > 0$ (**B**) observed over Toolik lake in 2015, with 95% confidence intervals.

1.2 Tables

Table S1. Long-term monitoring variables from the LTER dataset available for trend analyses during the past 30+ years of observation. For the detailed sensor history see https://toolik.alaska.edu/edc/monitoring/abiotic/weather.php?tab=metadata.

Variable	Height	Since	Resolution	Comment
Air temperature*	5 m	25 Jun 1988	1 h	
Barometric pressure		16 Jun 1990	1 h	
Global radiation		10 Jun 1988	1 h	(short-wave incoming radiation)
Lake depth		16 Aug 1989	3 h	
Lake temperature		12 Jun 1988	3 h	
Rain		10 Jun 1988	1 h	
Relative humidity*	5 m	25 Aug 1988	1 h	
Snow depth		14 Nov 2014	3 h	not used here
Soil temperatures	0.00 (moss), –0.05, –0.10, –0.20, –0.50, –1.00, –1.5 m	15 Jun 1988 to 18 Aug 1998	3 h	
Vapor pressure deficit		16 Jun 1990	1 h	calculated
Wind direction	5 m	25 Aug 1988	1 h	not used here
Wind speed	5 m	25 Aug 1988	1 h	

* in the early years there were problems with the sensors. Until 16 June 1996 the original EDC dataset has been corrected using a linear regession with data from two nearby sites (WSG89 and MAT89 sites; Laundre pers. comm.). In case of relative humidity the sensor saturated below 100% until it was replaced on 16 June 1996. We thus applied an offset correction, taking the centered moving 7-day average maximum relative humidity as the 100% reference (see Figure S5).

Table S2. Best fits to Toolik Lake data from Figures; best estimate ± standard error of fit.

	a	b	c	d	e	g
	1	**x**	**x^2**	**x^3**	**x^4**	**x^6**
Figure 6A	1.29 ± 0.50	0.94 ± 0.33	-0.180 ± 0.051			
Figure 6B	0.0140 ± 0.0021	0.00853 ± 0.00074	— ± —	— ± —	— ± —	0.00000047 ± 0.00000008
Figure 6C	3.33 ± 0.37	-8.5 ± 2.9	— ± —	8.3 ± 10.7		
Figure 6D	2.22 ± 0.82	-5.2 ± 8.6	16.1 ± 17.3			
Figure 7A	1.45 ± 0.34	-0.024 ± 0.066	— ± —	— ± —	0.000220 ± 0.000033	
Figure 7B	0.0364 ± 0.0019	-0.00214 ± 0.00057	-0.000175 ± 0.000049			
Figure 8A	45.9 ± 3.4	-1.26 ± 0.38				
Figure 8B	11.29 ± 0.71	0.918 ± 0.079				
Figure 9A	1.96 ± 0.18	0.005 ± 0.011	— ± —	-0.0000131 ± 0.0000052		
Figure 9B	0.0490 ± 0.0052	-0.00049 ± 0.00021	— ± —	— ± —	— ± —	2.088E-12 ± 4.845E-13
Figure 10A	0.0759 ± 0.0013	0.004694 ± 0.000095				

Table S3. Equations used in Figure 7 that relate K600 piston velocity (cm h^{-1}) to the wind speed (U) at 10 meters height, (U10 in m s^{-1}).

Reference	**Equation**
Cole and Caraco (1998)	$K600 = 2.07 + 0.215 \cdot U10^{1.7}$
Crusius and Wanninkoff (2003)	
U10 < 3.7 m s^{-1}	$K600 = 0.72 \cdot U10$
U10 ≥ 3.7 m s^{-1}	$K600 = 4.33 \cdot U10 – 13.3$
Frost & Upstill-Goddard (2002)	$K600 = 0.679 \cdot R – 0.0015 \cdot R^2 + 0.929$
R = rainfall in mm h^{-1}	
Guérin et al. (2007)	
Linear	$K600 = 0.9 \cdot U10 + 1.29$
Power	$K600 = 1.69 + 0.33 \cdot U10^{1.59}$
Exponential	$K600 = 1.61 \cdot e^{0.26 \cdot U10}$
Ho et al. (2006)	$K600 = 0.266 \cdot U10^2$
Liss and Merlivat (1986)	
U10 ≤ 3.6 m s^{-1}	$K600 = 0.17 \cdot U10$
3.6 < U10 ≤ 13 m s^{-1}	$K600 = 2.95 \cdot U10 – 9.65$
U10 > 13 m s^{-1}	$K600 = 5.9 \cdot U10 – 49.3$
MacIntyre et al. (2010)	$K600 = 2.25 \cdot U10 + 0.16$